Full dynamics of a red blood cell in shear flow

Jules Dupire, Marius Socol, and Annie Viallat[1]

Aix Marseille Université, Centre National de la Recherche Scientifique, Laboratoire Adhésion et Inflammation Unité Mixte de Recherche 7333, Inserm UMR1067, 13009 Marseille, France

Edited by T. C. Lubensky, University of Pennsylvania, Philadelphia, PA, and approved October 30, 2012 (received for review June 20, 2012)

At the cellular scale, blood fluidity and mass transport depend on the dynamics of red blood cells in blood flow, specifically on their deformation and orientation. These dynamics are governed by cellular rheological properties, such as internal viscosity and cytoskeleton elasticity. In diseases in which cell rheology is altered genetically or by parasitic invasion or by changes in the microenvironment, blood flow may be severely impaired. The nonlinear interplay between cell rheology and flow may generate complex dynamics, which remain largely unexplored experimentally. Under simple shear flow, only two motions, "tumbling" and "tank-treading," have been described experimentally and relate to cell mechanics. Here, we elucidate the full dynamics of red blood cells in shear flow by coupling two videomicroscopy approaches providing multidirectional pictures of cells, and we analyze the mechanical origin of the observed dynamics. We show that contrary to common belief, when red blood cells flip into the flow, their orientation is determined by the shear rate. We discuss the "rolling" motion, similar to a rolling wheel. This motion, which permits the cells to avoid energetically costly deformations, is a true signature of the cytoskeleton elasticity. We highlight a hysteresis cycle and two transient dynamics driven by the shear rate: an intermittent regime during the "tank-treading-to-flipping" transition and a Frisbee-like "spinning" regime during the "rolling-to-tank-treading" transition. Finally, we reveal that the biconcave red cell shape is highly stable under moderate shear stresses, and we interpret this result in terms of stress-free shape and elastic buckling.

elastic capsule | low Reynolds number | shape memory | erythrocyte

Blood is a concentrated suspension of cells: 45% in volume is occupied by red blood cells (RBCs). Its fluidity strongly depends on its behavior in flow, which is a key factor of proper tissue perfusion. At the cellular scale, blood flow behavior is affected primarily by the RBC response to the hydrodynamic stress in terms of cell orientation relative to the flow direction and of cell deformation. For example, on one hand, at low shear rates, similar cell orientations may favor the formation of stacks (rouleaux) (1) of RBCs, like rolls of coins, which increases blood viscosity. On the other hand, at high shear rates, the individualization of RBCs, their alignment, and their stretching in the flow (2) decrease blood viscosity (3). The orientation and the deformation in flow of RBCs are governed by their rheological properties. They result from the viscoelastic contributions of all components of the cell composite structure. Moreover, RBC rheological properties also depend on the microenvironment and on metabolic functionality (4). Both local and systemic disturbances of homeostasis (in diabetes mellitus, hypertension) have the potential to induce RBC rheological alterations and consequently to impair blood circulation. It therefore is crucial to understand the relationships between the rheological properties of RBCs and their orientation and deformation in flow. This question is far from trivial because even in a simple shear flow, RBCs present a variety of dynamic states, such as steady tank-treading, swinging, unsteady tumbling, and chaotic motion.

To date, there has been little experimental work on the connection between the mechanical properties of RBCs and their dynamics in shear flow (5–8), compared with the many numerical and theoretical recent studies reported for capsules (9–11) and red blood cells (12–16). Surprisingly, all investigations dealing with RBC orientation in flow focus on a very particular case in which the axis of symmetry of the cell lies in the shear plane. Some observations, however, suggest that other cellular orientations may be more stable (17, 18). Furthermore, numerical predictions of RBC deformations show significant discrepancies with experimental observations. Indeed, experiments report only the stationary stretched shape of cells steadily aligned in the flow at high shear rates, whereas recent numerical studies predict "breathing" dynamic states with strong shape deformations at low shear rates for both RBCs and elastic capsules (9–16).

Here, we couple two videomicroscopy approaches providing multidirectional pictures of RBCs to elucidate the full dynamics of an RBC in shear flow, and we analyze the mechanical origin of the observed dynamics (shapes and regimes of motion).

Under physiological conditions, a mature cell is a biconcave disk about 6–8 μm in diameter and 2 μm thick. Its membrane consists of a fluid lipid bilayer and an elastic spectrin network lying just beneath the bilayer and attached to the membrane integral proteins. The inner cell volume is filled with a solution of hemoglobin. Although the structure of the RBC is one of the simplest among cells, it nevertheless involves several mechanical parameters: viscosities of the hemoglobin solution and of the lipid bilayer, incompressibility and bending elasticity of the lipid bilayer, and compressibility and shear elasticity of the spectrin cytoskeleton. The nonspherical biconcave shape of RBCs enables shape changes at constant volume and area. Moreover, the membrane has a memory of its shape (19): after a shape deformation induced by an external force, the membrane returns to its initial biconcave shape and the membrane elements return to their initial position after removal of the force. The rim, for instance, is always formed by the same membrane elements. However, the actual deformation state of the membrane, even in the biconcave state, is not known because the stress-free shape of the membrane for which the strain energy vanishes, has not been determined.

For many years, the viscosity ratio λ, where λ is the viscosity inside the cell relative to the viscosity of the suspending solution, has been the only mechanical parameter used to describe the behavior of RBCs in shear flow observed in pioneering studies (2, 20): at high λ, RBCs have been reported to tumble (T), referred to here as the particular unsteady flipping motion (F) when the cell axis of symmetry rotates in the shear plane. The nature of this motion (rigid-body–like or with membrane movement) and its stability are not experimentally known. At low λ values and high shear rates, RBCs have a "fluid-like" tank-treading movement in which the membrane rotates around the center of mass of the cell and has a quasi-stable inclination (TT). The Keller and Skalak (KS) analytical model (21), which describes an RBC as a viscous ellipsoid of fixed shape, qualitatively recovers (T), (TT) as a function of λ. However, recent experiments revealed new dynamic states specifically due to the shear elasticity and the shape memory of the red cell membrane (7, 8): (*i*)

Author contributions: A.V. designed research; J.D. and M.S. performed research; J.D., M.S., and A.V. analyzed data; and J.D. and A.V. wrote the paper.

The authors declare no conflict of interest.

This article is a PNAS Direct Submission.

[1]To whom correspondence should be addressed. E-mail: annie.viallat@inserm.fr.

This article contains supporting information online at www.pnas.org/lookup/suppl/doi:10.1073/pnas.1210236109/-/DCSupplemental.

Downloaded by guest on February 24, 2022

swinging superimposed to tank-treading, in which the cell's inclination angle changes periodically relative to the direction of flow (S); (*ii*) *intermittency*, in which the cell alternately Ts and TTs when it undergoes a TT-to-T transition driven by the shear rate, $\dot{\gamma}$; and (*iii*) *chaotic motion* in a time-periodic flow (8). The KS model modified to account for membrane elasticity and shape memory, developed by Abkarian et al. (AFV) (7) and by Skotheim and Secomb (SS) (14), semiquantitatively recovers these dynamic states and their transition. Since then, this field has been very active and many theoretical and numerical approaches have been developed (9–16), which account for the most important cell mechanical parameters and allow shape deformation. They recover the various regimes of motion, except intermittency, which is still controversial, but also predict new regimes associated with strong unsteady deformations that have never been seen experimentally. Moreover, probably for the sake of simplicity, all studies ignore the motion of the cell when its initial orientation is random with respect to the shear plane.

In this paper, we report the following: (*i*) In contrast to the common belief that the stable RBC motion at low $\dot{\gamma}$ is tumbling, we show that the RBC orientation in flow changes when $\dot{\gamma}$ increases, until the cell rolls steadily (R), similar to a wheel on a road. This dynamic state preserves the cell from energetically costly deformations and is a true signature of the elasticity of the cytoskeleton. (*ii*) The RBC dynamic states display a hysteresis with $\dot{\gamma}$. Upon decreasing $\dot{\gamma}$, the tank-treading-to-flipping transition occurs via a transient intermittent regime. Upon increasing $\dot{\gamma}$, flipping evolves to rolling and the transition to tank-treading occurs via a transient Frisbee-like spinning motion, which we describe. for the first time. (*iii*) Contrary to most numerical simulations, RBC shapes do not present strong periodic "breathing" deformations in the tank-treading/swinging regime at moderate shear stress and remain biconcave. We discuss the stress-free shapes of RBCs that might explain the stability of their biconcave shape in terms of elastic buckling. This shape stability suggests that the shape-preserving analytical model (AFV-SS) is suitable to describe the dynamics of RBCs in the tank-treading/swinging regime. It opens the way to observations that allow simultaneous assessment of membrane shear modulus and viscosity, and hold promise for applications in cellular-scale diagnostics in clinical hemorheology.

Results

We first describe the dynamics of RBCs in the flipping rigid-body–like regime. We explore regimes of motion, orbits, and deformations. We describe the cell dynamic states during the two transitions toward the fluidized dynamic state and toward the solid dynamic state. We finally discuss the role of the cell mechanics on the observed dynamics.

Nonfluidized Regimes: From Tumbling to Rolling. RBCs are diluted in 9% (wt/wt) PBS–dextran solutions for two molecular weights of dextran, 10^5 g/mol (of viscosity η = 7.15 mPa·s) and 2×10^6 g/mol (η = 28.5 mPa·s). Some additional experiments are done with RBCs diluted in 7.5% (wt/wt) (η = 22.2 mPa·s) and 4% (wt/wt) (η = 7.8 mPa·s) solutions of PBS and 2×10^6 g/mol dextran. Individual RBCs are first introduced in a flow chamber, then are subjected to a simple shear flow and observed. The shear rate $\dot{\gamma}$ is increased by steps from 0 to 15 s^{-1} for cells suspended in dextran 10^5 g/mol and to 2.7 s^{-1} for cells suspended in 9% (wt/wt) dextran 2×10^6 g/mol. In this case, above $\dot{\gamma} = 2.7\ s^{-1}$, cells tank-tread. Initially, RBCs present various initial orientations with respect to the flow direction, but we focus more specifically on the cells for which the initial angle of the cell axis of revolution is in the shear plane. The cell motion, although periodic, at first sight appears rather complex and similar to that described by Jeffery (22) for rigid ellipsoids. We characterize the cell orientation by two angular variables: the *orbit angle*, ϕ, between the orthogonal projection of the cell axis of revolution along the flow gradient and the flow direction, and the *cell inclination angle*, θ, between the orthogonal projection of the cell axis of revolution onto the shear plane and the flow gradient direction (Fig. 1*A*).

Cell orbit. The orbit angle is best detected by observations along the flow gradient (*z*-view). The cell rocks to and fro between the orbit angles $\pm\ \phi$ observed when the cell is on the edge (axis of revolution perpendicular to the flow gradient). At low shear rates and starting from low ϕ values (close to tumbling motion), the first striking result is that ϕ does not remain constant. It fluctuates between 0° and 40° but never exceeds 40°. When the shear rate increases, the orbit of the cell drifts and ϕ increases and reaches a well-determined limiting value, which depends on the shear rate. This result is illustrated in Fig. 1*B* and Movie S1. It is shown in Fig. 2 on 18 different cells, whose orbit has been measured at several increasing shear rates. The cell spins around

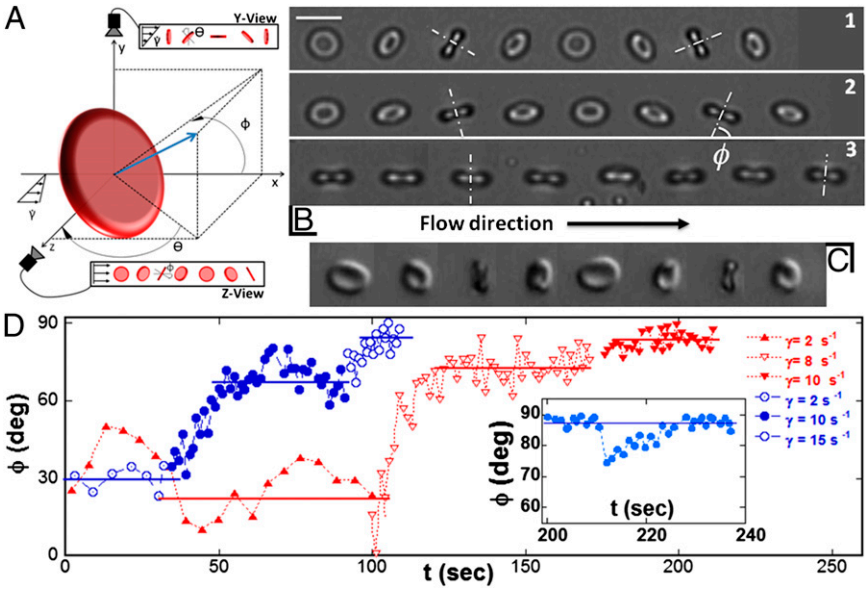

Fig. 1. Orbit change of flipping RBCs in a shear flow when the shear rate increases. Observations along the flow gradient (*z*-view). (*A*) Schematic drawing. (*B*) Flipping of one RBC in dextran solution [10^5 g/mol, concentration (c) = 9% (wt/wt)]. (*B*, *1*) $\dot{\gamma} = 2\ s^{-1}$, time sequence of 10.6 s. (Scale bar, 10 μm.) (*B*, *2*) $\dot{\gamma} = 6\ s^{-1}$, time sequence of 3.72 s. (*B*, *3*) $\dot{\gamma} = 12\ s^{-1}$, time sequence of 3.84 s. (*C*) Flipping of a hardened RBC at $\dot{\gamma} = 15\ s^{-1}$, time sequence of 1.2 s (DIC image). (*D*) Temporal increase and stabilization of the angle φ when the shear rate is increased by step, observed on two RBCs (blue and red symbols, respectively) in dextran solution (10^5 g/mol, c = 9% (wt/wt)). The horizontal bars are the limit value of φ reached for a given shear rate. (*D*, *Inset*) Perturbation and recovery of the axis of revolution of an RBC. $\dot{\gamma} = 12\ s^{-1}$.

APPLIED PHYSICAL SCIENCES
BIOPHYSICS AND COMPUTATIONAL BIOLOGY
Downloaded by guest on February 24, 2022

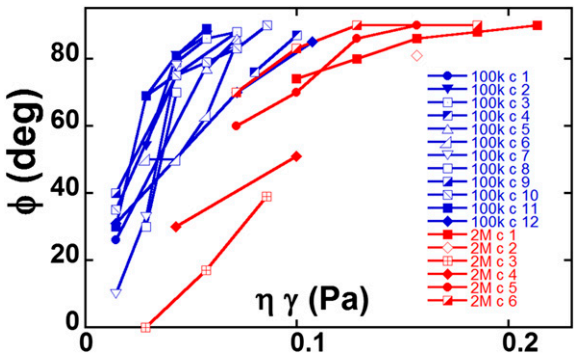

Fig. 2. Variation of the limit value of φ vs. the shear stress $\eta\dot{\gamma}$. Each symbol refers to a single cell suspended in solution [9% (wt/wt)] of dextran of molecular weight 10^5 g/mol (blue) or 2 10^6 g/mol (red).

its axis of revolution, which has a precession movement when the orbit departs from pure tumbling ($\phi = 0°$). When the cell orbit is perturbed, the angle ϕ recovers its stable value spontaneously (Fig. 1*D*, *Inset*). Upon further $\dot{\gamma}$ increase, the cell lies in the shear plane and rolls ($\phi = 90°$). This motion corresponds to a steady spin of the axis of symmetry about the vorticity axis (Fig. 1*B*). The variation of ϕ with the shear stress is shown in Fig. 1*D*, *Inset*. A small shift exists between the angle ϕ observed for RBCs suspended in dextran 2 10^6 g/mol and in dextran 10^5 g/mol, which we do not explain here.

To determine the mechanical origin of the phenomenon, we stiffened RBCs by incubating them in a solution of glutaraldehyde, which cross-links the proteins of the cell membrane. In this case, tumbling is stable even for $\dot{\gamma} = 15\ s^{-1}$ (Fig. 1*C*). ϕ may fluctuate but remains less than 40°, and returns to zero from time to time. When the orbit is perturbed externally up to $\phi = 50°$, ϕ returns to zero, clearly demonstrating that finite membrane elasticity promotes rolling whereas rigidity induces tumbling.

Cell inclination. The temporal evolution of the inclination angle θ of the cells imaged in the shear plane (*y*-view) is shown in Fig. 3*B*. Although the orbit changes when $\dot{\gamma}$ increases, θ is determined easily as long as the cell does not fully roll in the shear plane. The temporal variation of θ for a flipping rigid ellipsoid, derived from Jeffery (22), is given by the equation

$$\tan\theta = r.\tan\frac{\dot{\gamma}t}{r+r^{-1}}, \qquad [1]$$

where *r* is the cell axis ratio (length of the axis of symmetry to the length of the diametrical axis). We fit the experimental time variations of θ by the two-parameters equation $\tan\theta = A\tan(B\pi t)$, where *A* characterizes the variations of the flipping velocity during the motion and $1/B$ is the period for one half-rotation from $\theta = -90°$ to 90°. Fits are very satisfactory for all studied cells, as

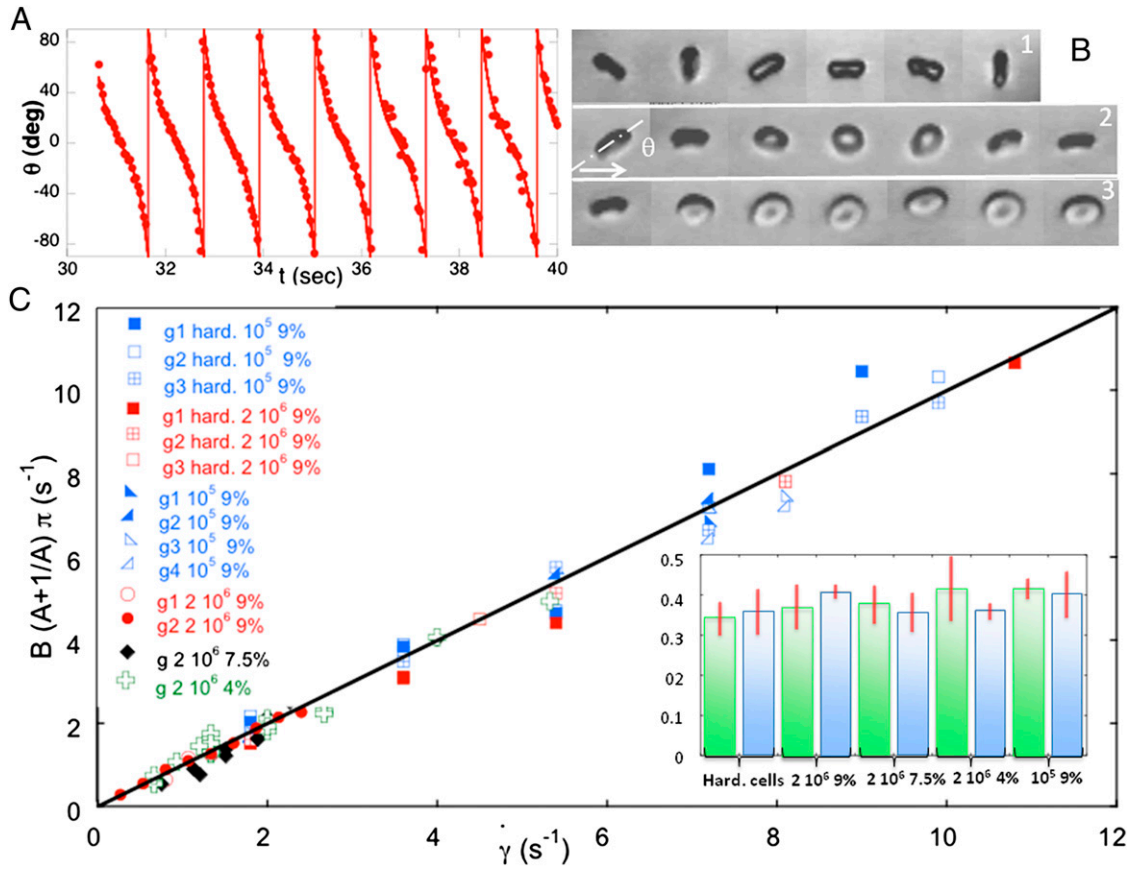

Fig. 3. Flipping of RBCs observed in the shear plane (*y*-view). (*A*) Experimental time variation of the inclination angle θ ($\dot{\gamma} = 9\ s^{-1}$) and fit by the function $\tan\theta = A\tan(B\pi t)$ (solid curve). (*B*) Variation of the orbit of one flipping RBC with increasing shear rate [dextran 2 10^6 g/mol, c = 9% (wt/wt)]. (*B*, *1*) $\dot{\gamma} = 2\ s^{-1}$, time sequence of 10.6 s. (*B*, *2*) $\dot{\gamma} = 6\ s^{-1}$, time sequence of 13.72 s. (*B*, *3*) $\dot{\gamma} = 12\ s^{-1}$, time sequence of 3.84 s. (*C*) Variation of the product $\pi B(A + 1/A)$with the shear rate, where *A* and *B* are determined from the fit: $\tan\theta = A\tan(B\pi t)$. The variation is in agreement with Jeffery and KS laws (solid line: bisector). (*C*, *Inset*) Histogram of values of *A* obtained by the fits for RBCs in various conditions. Stiffened and normal cells in dextran 10^5 g/mol, c = 9% (wt/wt) (green) $\dot{\gamma} < 5\ s^{-1}$, (blue) $\dot{\gamma} > 5\ s^{-1}$. Cells in dextran 2 10^6 g/mol, c = 9% and 7.5%: (green) $\dot{\gamma} < 1.34\ s^{-1}$, (blue) $\dot{\gamma} > 1.34\ s^{-1}$.

Downloaded by guest on February 24, 2022

illustrated in Fig. 3*A*. To interpret *A* and *B* parameters according to Eq. **1**, we show on 14 stiffened and normal cells, under various shear rates and in solutions of dextran 10^5 g/mol or 2 10^6 g/mol ranging from 4% to 9% (wt/wt), that $\pi B(1/A+A)$ values plotted versus $\dot{\gamma}$ lie on the bisectrix, as expected from Eq. **1** (Fig. 3*C*). The values of *A* shown in Fig. 3*C*, *Inset*, then, are expected to be equal to the cell axis ratio, *r*. Indeed, they all are in the same range, whatever the shear stress and the cell rigidity (stiffened cells are expected to move as rigid ellipsoids), and are in agreement with both the value $r = 0.38$, found long ago by Goldsmith and Marlow (20) from fitting RBC tumbling, and the actual axis ratio of RBCs measured at rest.

However, as is well known, the RBC membrane is not rigid. We need a more refined discussion. We first stress that the cell shape deformation is small during the motion, so we focus our result analysis in light of shape-preserving models. Indeed, the temporal variation of θ for a tumbling fluid ellipsoid described by KS also obeys Eq. **1**, with *r* depending on the viscosity ratio. In this case, the material points are not fixed on the membrane. They oscillate on the ellipsoidal shape and slowly drift in a very slow tank-treading motion (fluid tumbling). Here, however, KS is clearly not valid because it predicts that cells suspended in 2 10^6 g/mol dextran should tank-tread for all $\dot{\gamma}$, although we observe that they flip at low $\dot{\gamma}$. More interesting is KS modified to account for elastic energy and shape memory (AFV and SS). At low shear rate, the material points are predicted to oscillate on the membrane but do not drift in a TT motion. Indeed, during TT, the membrane elements undergo a strong local shear deformation while rotating from the rim to the dimple of the cell. This strain involves an energy too high to be provided by the external flow at low shear rate. The temporal variation of θ during this elastic tumbling therefore is generally similar to that of a rigid ellipsoid. When the shear rate increases, the work provided by the flow allows large amplitude of oscillation of the points on the membrane. Beyond a critical shear rate, the work done by the flow is sufficient to overcome the barrier of strain energy required for complete rotation of the membrane: the membrane is fluidized. Either tank-treading or fluid tumbling, as described by KS, then is expected to occur, depending on the viscosity ratio. The observations reported here clearly indicate the following: (*i*) At low shear rate, the cell motion is similar to a rigid ellipsoid, likely with very small oscillations of the membrane elements associated with a small shear strain of the membrane. (*ii*) When the shear rate increases, the increase of amplitude of oscillations of the position of the membrane elements destabilizes the orbit of the cell movement. The change of the orbit allows limiting of the local shear deformations of the membrane and likely the overall cell shape deformation. (*iii*) Finally, the cell rolls (no shear deformation) before the critical shear rate of "fluidization" is reached.

Shape deformation. We emphasize again that the cell shape is preserved during the whole motion regardless of the cell orientation. Cells remain biconcave disks, with a thickness that does not change significantly. The length variation of the long cell axis is less than 10% for the entire studied range of shear stresses (0–0.25 Pa), as shown in Figs. 1 (sequences) and 2 (sequence and *r* are the same for all shear stresses).

In the Jeffery model (22), all orbits of a flipping cell are possible. Here, RBCs present specific orientations in flow, which seem to be determined by the capillary number $Ca = \eta a\dot{\gamma}/\mu$, where μ is the shear deformation modulus of the cytoskeleton and *a* is the RBC size. Stiffened cells ($Ca = 0$) tumble, as has been observed for rigid disks (23). This motion corresponds to the least dissipation of energy. The orbit angle of flipping viscoelastic cells changes when *Ca* increases, when $\dot{\gamma}$ increases. As the shear stress reaches 0.1–0.2 Pa, the cells roll, as already reported by Bitbol (17) and Watanabe et al. (18). This motion, similar to a solid rotation, corresponds to a minimum of membrane shear strain energy. Therefore, the orientation of the cell seems to be governed by a compromise between viscous dissipations in the system and the shear strain energy. The very small shape deformation suggests that the loss of the biconcave disk shape requires even more energy. This point is discussed later.

From and Toward Fluidized Regime. Below the threshold of the viscosity ratio and above a critical value of the shear rate, RBCs have a fluidized regime with swinging (S) and tank-treading (TT) motion (Fig. 4*A*, *z*-view). We explore the transition from fluidized to nonfluidized regimes and from nonfluidized toward fluidized regimes by cyclically decreasing and increasing the shear rate.

From tank-treading to flipping. The transition is observed along the flow gradient by decreasing $\dot{\gamma}$ below a critical value $\dot{\gamma}_c^-$. At the transition, the cell exhibits a transient intermittent regime, as illustrated in Fig. 4*B*. One or one-half a swinging/tank-treading period and one or two flips characterized by a small value of the orbit angle ϕ (tumbling motion) are observed successively. The intermittent regime finally stops when the flips occur with an orbit angle larger than 40°. Then, the cell starts to flip continuously with a given orbit ϕ, which tends toward the stable ϕ-angle associated with the applied $\dot{\gamma}$. This behavior is shown in Fig. 4*C*. Then, we increase $\dot{\gamma}$ and observe a progressive rotation of the cell orbit until the cell rolls.

Cell deformation during the TT–F transition. As shown in Fig. 4 *A* and *B* and Movie S2 by differential interference contrast (DIC) and phase contrast microscopy, RBCs present a stationary biconcave shape during S and TT and are not significantly deformed. The

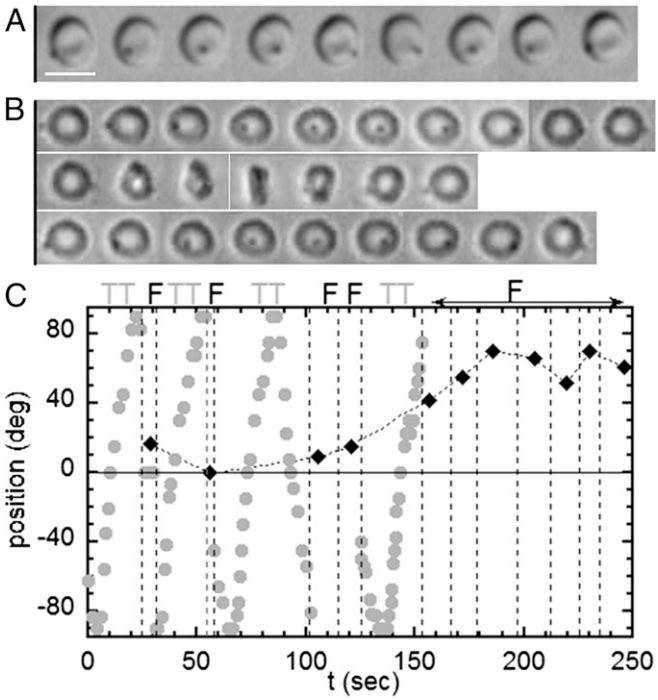

Fig. 4. Tank-treading-to-flipping transition of RBCs whose membrane bears a latex bead (diameter, 1 μm); dextran 2 10^6 g/mol, c = 9% (wt/wt); scale bar, 8 μm; top-view observation. (*A*) Tank-treading RBC with rotation of the bead. The dimple of the biconcave shape is preserved (DIC image), $\dot{\gamma} = 3\ s^{-1}$, time sequence of 5.48 s. (*B*) Intermittency at the transition. Sequences show TT, F, and TT, respectively; $\dot{\gamma} = 0.8\ s^{-1}$; time sequence of 47.84 s. Tank-treading is detected from the rotation of the bead. The cell is still biconcave with the presence of the dimple (phase contrast image). (*C*) Transient intermittency. Dotted lines separate tank-treading from flipping regimes. ●, Variation of the bead position between −90° (1st image) to +90° (10th image) vs. time during the tank-treading–flipping transition at $\dot{\gamma} = 0.8\ s^{-1}$. ♦, Values of the angle φ during the flipping; when φ reaches 40°, the flipping regime is stabilized.

APPLIED PHYSICAL SCIENCES
BIOPHYSICS AND COMPUTATIONAL BIOLOGY
Downloaded by guest on February 24, 2022

length variation of the long cell axis is less than 10% for the entire studied range of shear stresses. This behavior was not highlighted in previous experimental studies, but previously published pictures already suggested it (7, 18). We show it clearly by visualizing on the same sequence the rotation of a small bead attached to the membrane and the presence of a dimple on the shape. Again, it is in contradiction with the numerical simulations that show strong nonstationary deformation on TT cells close to the transition (12, 13, 24).

From rolling to tank-treading. The R–S-TT transition is induced by further increasing $\dot{\gamma}$ above a critical value $\dot{\gamma}_c^+$. All steps of the transition are illustrated in Fig. 5*A* using a bead attached to the cell membrane to visualize the motion of the membrane. Starting from rolling in the shear plane, the cell progressively tilts and hovers in the flow while its membrane spins around the axis of revolution. This one does not precess during the motion and rises slowly by turning around the direction of the flow. The cell motion looks like a flying Frisbee, although there is no inertial effect. Finally, after a rotation of 90°, the axis of revolution arrives in the shear plane and the cell lies perpendicular to the shear plane. Tank-treading occurs when the streamlines on the membrane change from circular spinning around the axis of revolution to tank-treading, i.e., a back-and-forth motion along the flow direction. This drastic change of motion is achieved without strong shape deformation, as shown in Fig. 5*A* and Movie S3. However, often one observes parts of the membrane that rotate as if they were not fluidized: a small solid section is embedded in the fluidized part and moves as a whole. Typical triconcave deformations are shown in Fig. 5*B* and Movie S4. The shapes obtained are very similar to knizocytes observed in newborns (25) or in patients with lecithin/cholesterol acyltransferase deficiency (26), and are attributed to impaired membrane deformability and fluidity. This suggests that at the critical $\dot{\gamma}_c^-$ value, the transition toward a fluidized dynamic regime of the cell is still incomplete and the RBC behaves like a cell with unpaired deformability. When $\dot{\gamma}$ is increased further, the cellular deformation disappears and the cell recovers its biconcave shape. Several hysteresis cycles of shear rate have been performed on a cell, during which $\dot{\gamma}$ decreased from above $\dot{\gamma}_c^+$ to below $\dot{\gamma}_c^-$ and then increased to above $\dot{\gamma}_c^+$ again. Both transitions always occur at the same value of $\dot{\gamma}_c^-$ and $\dot{\gamma}_c^+$.

The transition between rigid-body–like and fluidized cell occurs in a hysteretic domain of shear rates, $\{\dot{\gamma}_c^- - \dot{\gamma}_c^+\}$. In this domain both flipping/rolling and tank treading are stable, each dynamic state depends on how it is reached, either by increasing or decreasing $\dot{\gamma}$. The mechanisms of transition toward F and toward TT are different. In the TT-to-F transition, TT stabilizes the cell orbit. In the R-to-TT transition, the cell axis of symmetry has to rotate through a $\pi/2$ angle. The streamlines on the cell membrane have to change abruptly with a sharp increase of shear strain energy. This can be achieved only at a higher shear rate value.

Finally, the values found for the critical shear stresses $\eta_0\dot{\gamma}_c^-$ (0.023 Pa) and $\eta_0\dot{\gamma}_c^+$ (0.086 Pa) are in agreement with that reported in ref. 7.

Final Discussion and Conclusion

It is important to note that although the biconcave shape of the membrane remains unchanged for the shear flows we have studied, the constitutive material elements of the membrane generally are strained on the biconcave surface. Even in the absence of flow, a material element may be strained if the biconcave shape is not the stress-free shape. When subjected to the flow, a material element is displaced on the biconcave surface and its strain varies as a result of the anisotropic shape of the membrane. Furthermore, RBCs have a shape memory, which means that the material elements of the membrane are not equivalent. Therefore, the local strain at a given position of the biconcave shape depends on the material element, which occupies this position at the considered instant. Consequently, the total shear strain energy of the membrane, defined as the sum of the local strain energies of the material elements, generally is not equal to zero. It varies over time, depending on the position of the material elements on the surface. A question then arises: Is the membrane strain energy related to the RBC orientation and motion in flow? If one considers the tumbling motion, the amplitude of the local displacement of the material elements on the surface increases with the shear rate, and so does the strain energy, for instance when the elements initially at the rim approach the dimple. However, when the cell orbit drifts toward rolling, the strains due to displacements on the surface decrease progressively and vanish when the axis of revolution is equal to the axis of rotation of the cell (rolling). Indeed, in the latter case, the cell has a solid rotational motion: a membrane material element always occupies the same position on the surface so that the total strain energy remains constant and equal to its value in absence of flow. The observed orbit change therefore seems to be an efficient means to prevent the increase of the total membrane strain energy with the shear rate at the cost of a higher external viscous dissipation. Similarly, the R–TT transition occurs at a shear rate higher than the TT, because R stabilizes the motion by minimizing the total strain energy.

Finally, the absence of significant cell shape deformation is puzzling, especially in the case of TT, when the hydrodynamic energy provided by the flow is high enough to strain the material elements of the membrane when they circulate on the biconcave shape. In this case, one may wonder what the energy is that enables a material element to deform locally to form a dimple, because hydrodynamic constraints tend to profile global ellipsoidal shapes, as observed for lipid vesicles or elastic capsules in flow. We propose an interpretation involving a buckling phenomenon for which the biconcave shape is of minimal energy, and a weak shape memory. The shape memory results from an anisotropic stress-free shape of the membrane. The anisotropy may come from the inhomogeneity of the spherical shell—for instance, strengthened equatorial region or anisotropic elastic properties (27)—or from a nonspherical shell. The latter hypothesis, supported by the work of Lim, Wortis, and Mukhopadhyay (28), allows one to find observed RBC shapes by using a mechanical model including bending, stretch, and shear elasticity.

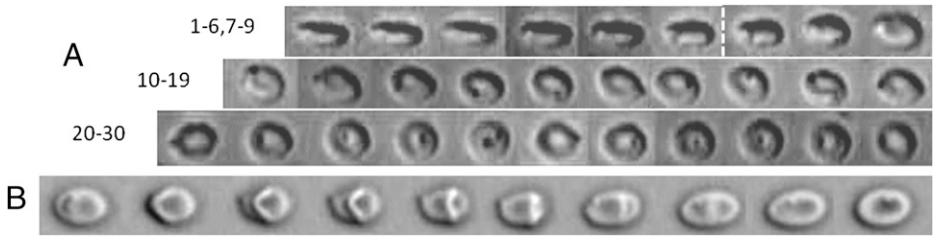

Fig. 5. Rolling-to-tank-treading transition observed on RBCs bearing a bead; dextran 2 10^6 g/mol, c = 9% (wt/wt); scale bar, 8 μm; top-view observation. (*A*) Shear rate = 3 s^{-1}. The symmetry axis of the rolling cell (images 1–7) rotates gradually (images 8–10). The spinning about the symmetry axis is detected by the bead motion (images 10–19). Finally, the streamlines change and the cell tank-treads (images 20–30). A vertical bar separates the different movements. Sequence of 46.6 s; scale bar, 7 μm. (*B*) The tank-treading movement at the transition sometimes presents an overall rotation of part of the membrane, which behaves locally like a solid by rotating as a whole. $\dot{\gamma}$ = 6 s^{-1}, time sequence of 1.98 s.

Downloaded by guest on February 24, 2022

According to their results, the stress-free shape of the RBC membrane is an ellipsoid of small eccentricity, with an area equal to that of an RBC and a volume, V, close to that of a sphere: the ratio V/V_{sphere} is in the range 0.989–0.95. Reducing the volume to the actual physiological RBC volume buckles the initial ellipsoid while keeping the area constant with apparition of two dimples in the polar regions. The material elements located at the initial equatorial region likely are located preferentially at the rim of the buckled biconcave shape, which then has a shape memory. However, because the anisotropy of the initial stress-free shape is small, the barrier of strain energy to displace the material elements from the rim to the dimple is low and will be overcome by providing a small hydrodynamic energy (low shear rates). Within this framework, a normal biconcave RBC shape may be considered as a buckled shell, in which the material elements of the membrane are strained at rest and have a small shape memory. We believe this biconcave shape remains that of lowest strain energy upon TT because of the low variation of strain energy upon displacement of the material elements, as long as the shear stress remains moderate. This shape will change progressively into an ellipsoidal shape at higher shear stresses, as observed by Fischer et al. (2).

We have shown that the shear elasticity of the RBC membrane is of foremost importance for cell deformation, motion, and orientation in shear flow. We observe that close to the transition $\dot{\gamma}_c^-$, the tumbling regime is unstable and we highlight the stable regime of rolling, in which the cell spins in the shear plane and rolls on its edge. Our results raise new questions about the behavior of viscoelastic particles in a viscous fluid at very low Reynolds number. Future models and simulations on RBCs should consider that the axis of revolution of the cell does not necessarily lie in the shear plane. Whether the observed orientational behavior can be explained by the minimum energy dissipation, as speculated by Jeffery, is still an open question, and we hope our work will stimulate new theoretical numerical studies. We also hope it will generate works on the strain energy of tank-treading buckled shapes of elastic capsules, starting from a quasi-spherical spheroid stress-free shape. Finally, the high stability of the biconcave RBC shape makes analytical shape-preserving models (AFV, SS) very attractive. Such models may be used to determine the viscosity and shear elasticity of RBCs *at very low shear stresses*, by fitting the characteristics of their dynamics in shear flow: swinging or TT frequency, critical shear rate $\dot{\gamma}_c$, or orbital angle ϕ. Such an approach, which needs an infinitesimal amount of blood, requires only microscopic observation of flowing cells without any single-cell manipulation.

Materials and Methods

RBC and Solution. The solutions of dextran (from *Leuconostoc* spp., Sigma-Aldrich) were prepared by diluting the dextran powder into PBS prepared using Gibco PBS pH7.4 10× stock solution. Osmotic pressure and pH were adjusted to 290 mOsm and 7.4, respectively. Two dextran polymers, one of 2,000 kDa and the other of 100 kDa molecular weight, were used. The dextran concentrations used in this study were 4% (wt/wt), 7.5% (wt/wt), and 9% (wt/wt) for dextran 2 10^6 g/mol and 9% (wt/wt) for dextran 10^5 g/mol. The corresponding range of viscosity was 2–34 Pa·s. At the 9% (wt/wt) concentration, the buoyancy effects on the cell were reduced. Dissolution was done at room temperature during all-night stirring. Before each experiment, 1 μL of blood was extracted via fingertip needle prick and diluted in 10 mL of PBS–dextran solution. All observations were carried out within 2 h.

Attachment of beads (carboxyl latex, 0.8 μm; Invitrogen) onto the RBC membrane was achieved by first washing 1 μL of blood in 1 mL of PBS. The cells then were incubated in 1 mL of PBS + beads solution at 4 °C for 1 h before being washed and resuspended in the PBS–dextran solution.

RBC stiffening was achieved by cell incubation in 1 mL of 20 μg/μL glutaraldehyde solution at room temperature for 1 h. Incubated cells were then washed and resuspended in the PBS–dextran solution.

Flow and Microscopy. Fluid was driven by a syringe pump (11 Plus series, Harvard Apparatus) at a constant flow rate ranging from 100 to 1200 μL/min through a parallelepiped glass chamber (1 × 10 × 50 mm). The wall shear rate ranged between 1 and 12 s^{-1}. Cells were visualized by 40× (DIC) and 50× (brightfield) objectives on a Leica DMIRB microscope within 50 μm of the 10 × 50-mm wall. Experiments referred as "*z*-view" were done with the direction of observation along the flow gradient, the objective being oriented perpendicular to the 10 × 50-mm side of the flow chamber. So-called *y*-view observations were made with the direction of observation perpendicular to the shear plane (through the 1 × 50-mm side of the flow chamber, tilting the microscope 90°). Images were recorded with a Cohu video camera at 25 frames per second. Movies finally were processed either manually or using a Matlab routine to obtain the angular variables related to the cell position.

ACKNOWLEDGMENTS. The group truly thanks M. Abkarian for discussions and M. Faivre and A. Rabier for their experimental help. M.S. thanks the ANR for funding. The group belongs to the Centre National de la Recherche Scientifique consortium CellTiss.

1. Barshtein G, Wajnblum D, Yedgar S (2000) Kinetics of linear rouleaux formation studied by visual monitoring of red cell dynamic organization. *Biophys J* 78(5):2470–2474.
2. Fischer TM, Stöhr-Lissen M, Schmid-Schönbein H (1978) The red cell as a fluid droplet: Tank tread-like motion of the human erythrocyte membrane in shear flow. *Science* 202(4370):894–896.
3. Dintenfass L (1968) Internal viscosity of the red cell and a blood viscosity equation. *Nature* 219(5157):956–958.
4. Baskurt OK, Meiselman HJ (2003) Blood rheology and hemodynamics. *Semin Thromb Hemost* 29(5):435–450.
5. Tran-Son-Tay R, Sutera SP, Rao PR (1984) Determination of red blood cell membrane viscosity from rheoscopic observations of tank-treading motion. *Biophys J* 46(1):65–72.
6. Tran-Son-Tay R, Sutera SP, Zahalak GI, Rao PR (1987) Membrane stress and internal pressure in a red blood cell freely suspended in a shear flow. *Biophys J* 51(6):915–924.
7. Abkarian M, Faivre M, Viallat A (2007) Swinging of red blood cells under shear flow. *Phys Rev Lett* 98(18):188302.
8. Dupire J, Abkarian M, Viallat A (2010) Chaotic dynamics of red blood cells in a sinusoidal flow. *Phys Rev Lett* 104(16):168101.
9. Bagchi P, Kalluri RM (2009) Dynamics of nonspherical capsules in shear flow. *Phys Rev E Stat Nonlin Soft Matter Phys* 80(1 Pt 2):016307.
10. Kessler S, Finken R, Seifert U (2008) Swinging and tumbling of elastic capsules in shear flow. *J Fluid Mech* 605:207–226.
11. Walter J, Salsac A-V, Barthes-Biesel D (2011) Ellipsoidal capsules in simple shear flow: Prolate versus oblate initial shapes. *J Fluid Mech* 676:318–347.
12. Le DV (2010) Effect of bending stiffness on the deformation of liquid capsules enclosed by thin shells in shear flow. *Phys Rev E Stat Nonlin Soft Matter Phys* 82(1 Pt 2):016318.
13. Sui Y, Chew YT, Roy P, Cheng YP, Low HT (2008) Dynamic motion of red blood cells in simple shear flow. *Phys Fluids* 20(11): no. 112106.
14. Skotheim JM, Secomb TW (2007) Red blood cells and other nonspherical capsules in shear flow: Oscillatory dynamics and the tank-treading-to-tumbling transition. *Phys Rev Lett* 98(7):078301.
15. Fedosov DA, Pan WX, Caswell B, Gompper G, Karniadakis GE (2011) Predicting human blood viscosity in silico. *Proc Natl Acad Sci USA* 108(29):11772–11777.
16. Dodson WR, 3rd, Dimitrakopoulos P (2010) Tank-treading of erythrocytes in strong shear flows via a nonstiff cytoskeleton-based continuum computational modeling. *Biophys J* 99(9):2906–2916.
17. Bitbol M (1986) Red blood cell orientation in orbit C = 0. *Biophys J* 49(5):1055–1068.
18. Watanabe N, Kataoka H, Yasuda T, Takatani S (2006) Dynamic deformation and recovery response of red blood cells to a cyclically reversing shear flow: Effects of frequency of cyclically reversing shear flow and shear stress level. *Biophys J* 91(5):1984–1998.
19. Fischer TM (2004) Shape memory of human red blood cells. *Biophys J* 86(5): 3304–3313.
20. Goldsmith HL, Marlow J (1972) Flow behavior of erythrocytes, I. rotation and deformation in dilute suspensions. *Proc R Soc Lond B Biol Sci* 182:351–384.
21. Keller SR, Skalak R (1982) Motion of a tank-treading ellipsoidal particle in a shear flow. *J Fluid Mech* 120:27–47.
22. Jeffery GB (1922) The motion of ellipsoidal particles immersed in a viscous fluid. *Proc R Soc Lond, A Contain Pap Math Phys Character* 102:161–179.
23. Taylor GI (1923) The motion of ellipsoidal particles in a viscous fluid. *Proc R Soc Lond, A Contain Pap Math Phys Character* 102:58–61.
24. Yazdani AZK, Kalluri RM, Bagchi P (2011) Tank-treading and tumbling frequencies of capsules and red blood cells. *Phys Rev E Stat Nonlin Soft Matter Phys* 83(4 Pt 2):046305.
25. Ruef P, Linderkamp O (1999) Deformability and geometry of neonatal erythrocytes with irregular shapes. *Pediatr Res* 45(1):114–119.
26. Lesesve JF, Garçon L, Lecompte T (2012) Finding knizocytes in a peripheral blood smear. *Am J Hematol* 87(1):105–106.
27. Pinder DN (1972) Shape of human red cells. *J Theor Biol* 34(3):407–410.
28. Lim HW G, Wortis M, Mukhopadhyay R (2002) Stomatocyte-discocyte-echinocyte sequence of the human red blood cell: Evidence for the bilayer- couple hypothesis from membrane mechanics. *Proc Natl Acad Sci USA* 99(26):16766–16769.

APPLIED PHYSICAL SCIENCES
BIOPHYSICS AND COMPUTATIONAL BIOLOGY
Downloaded by guest on February 24, 2022